Wind and Structures, *Vol. 19, No. 3 (2014) 249-270*
DOI: http://dx.doi.org/10.12989/was.2014.19.3.249

Wind characteristics observed in the vicinity of tropical cyclones: An investigation of the gradient balance and super-gradient flow

K.T. Tse[1], S.W. Li[*2], C.Q. Lin[1] and P.W. Chan[3]

[1]*Department of Civil and Environmental Engineering, Hong Kong University of Science and Technology, Clear Water Bay, Kowloon, Hong Kong*
[2]*CLP Power Wind/Wave Tunnel Facility, The Hong Kong University of Science and Technology, Clear Water Bay, Kowloon, Hong Kong*
[3]*Hong Kong Observatory, 134A Nathan Road, Kowloon, Hong Kong*

(Received December 5, 2013, Revised May 19, 2014, Accepted June 16, 2014)

Abstract. Through comparing the mean wind profiles observed overland during the passages of four typhoons, and the gradient wind speeds calculated based on the sea level pressure data provided by a numerical model, the present paper discusses, (a) whether the gradient balance is a valid assumption to estimate the wind speed in the height range of 1250 m ~ 1750 m, which is defined as the upper-level mean wind speed, in a tropical cyclone over land, and (b) if the super-gradient feature is systematically observed below the height of 1500 m in the tropical cyclone wind field over land. It has been found that, (i) the gradient balance is a valid assumption to estimate the mean upper-level wind speed in tropical cyclones in the radial range from the radius to the maximum wind (RMW) to three times the RMW, (ii) the super-gradient flow dominates the wind field in the tropical cyclone boundary layer inside the RMW and is frequently observed in the radial range from the RMW to twice the RMW, (iii) the gradient wind speed calculated based on the post-landfall sea level pressure data underestimates the overall wind strength at an island site inside the RMW, and (iv) the unsynchronized decay of the pressure and wind fields in the tropical cyclone might be the reason for the underestimation.

Keywords: boundary layer height; field measurements; gradient balance; super-gradient feature; typhoon mean wind profile

1. Introduction

Being a major destructive force to society, tropical cyclones pose danger in hurricane-prone regions. In particular, the strong winds carried by a tropical cyclone may induce severe property damages, and in some cases even loss of life (Wang and Wu 2003). Understandably, a significant part of the damage results from the strong winds in the tropical cyclone boundary layer (TCBL). Given the importance of the wind field in the TCBL, a considerable number of published works have investigated the models used to calculate the mean wind speed in the TCBL. For example, Shapiro (1983) introduced a slab model, with a constant boundary layer height, to describe the asymmetry of the horizontal variation of the mean wind speed in the TCBL. As an extension,

*Corresponding author, Dr., E-mail: samli@ust.hk

http://www.techno-press.org/?journal=was&subpage=8 ISSN: 1226-6116 (Print), 1598-6225 (Online)

Kepert (2001) derived a model to describe both the horizontal and vertical variations of the mean wind speed in the TCBL. Under the similarity assumption, Foster (2009) theoretically extended the model by Kepert (2001) to depict the wind field in the TCBL when the turbulent mixing is modelled by more than a constant turbulence diffusivity coefficient.

It is worthwhile to point out that the models mentioned above calculate the wind speeds in the TCBL by assuming the gradient balance holds at a sufficiently high altitude. However, whether the gradient balance is a valid assumption in tropical cyclones is debatable. Willoughby (1990) investigated the gradient balance using in-situ observations obtained by research aircraft penetrating typhoons and tropical storms, and concluded that the azimuthally averaged upper-level wind speed was approximately in gradient balance. Gray (1991), on the contrary, showed that the gradient balance is not a valid assumption in tropical cyclones by plotting the observed wind velocities against the ratio between the actual radius and the radius to the maximum wind (RMW). More recently, Kepert (2006a,b) investigated two typhoons in-depth, using the direct measurements of wind velocities taken by the Global Positioning System (GPS) dropwindsondes, and concluded that, while the lower and middle troposphere in Hurricane George (1998) was in gradient balance, the gradient balance was not present in the wind field of Hurricane Mitch (1998). Although the gradient balance is an important and controversial assumption, and therefore has been intensively studied using the measurements taken over open waters, there is no systematic study, to the best of our knowledge, that has focused on the gradient balance in the tropical cyclone wind field over land.

Within the TCBL, the maximum wind speed is frequently found to be higher than the gradient wind velocity determined from the horizontal pressure variations. Such a feature is due to the super-gradient flow in the TCBL, for which Kepert (2001) has developed a theoretical model. Based on the GPS dropwindsonde measurements taken during 1997~2003, Vickery *et al*. (2009) suggested an empirical model to describe the vertical variation of the mean wind speed in the TCBL, which includes a description of the super-gradient wind velocity found below the gradient height. Through investigating the observations of the onshore mean wind profile in the TCBL obtained by remote sensing techniques, Tse *et al*. (2013) found that the empirical model suggested by Vickery *et al*. (2009) is not applicable to describe the vertical variation of the mean wind speed in the inland TCBL. In fact, the decreasing trend of the mean wind speed above the super-gradient flow, which was the motivation for Vickery *et al*. (2009) to develop the model, was not systematically observed in the onshore mean wind profiles in the TCBL. Since it is impossible to entirely eliminate the influence of inland topography in the investigation, Tse *et al*. (2013) argued that the internal boundary layer developed due to land terrains far away from the observation site may be the reason for the model suggested by Vickery *et al*. (2009) being inapplicable. The study of Giammanco *et al*. (2013), however, showed clearly that the super-gradient flow was observed for the inland wind profiles in the TCBL. As a result, it is necessary to further investigate, without the assistance of the empirical model of Vickery *et al*. (2009), the super-gradient flow in the inland TCBL wind field.

Using the wind measurements taken by a Doppler SODAR and a boundary layer wind-profiler (installed in an automated weather station in Hong Kong) during the passages of four typhoons from 2008 to 2009, the mean wind profiles in the inland TCBL were calculated. Both the Doppler SODAR and the boundary layer wind-profiler are meteorology observation equipment, which detect wind speeds and directions at various heights in the atmosphere. While a technical introduction of the Doppler SODAR and the boundary layer wind-profiler will be presented in section 2, it should be noted here that the measurements taken by the Doppler SODAR and the

boundary layer wind-profiler are fundamentally different from the measurements taken by conventional techniques, such as anemometers. In essence, the wind speed measurements taken by the Doppler SODAR and the boundary layer wind-profiler is temporal (within the scan interval) and spatial (within the resolved volume) mean values. The measurements taken by the anemometer, on the other hand, are considered instantaneous wind speeds.

At the same time as the mean wind profiles in the inland TCBL were calculated using wind velocity measurements taken by both the Doppler SODAR and the boundary layer wind-profiler, the sea level pressure data with the same time stamp as the mean wind profiles were provided by a numerical model. The sea level pressure was then fitted to an empirical model describing the horizontal variation of the tropical cyclone sea level pressure. Since the model also contains a description of the horizontal variations of the gradient wind speed, the gradient wind speed at the measurement site was calculated using the parameters derived from fitting the sea level pressure data. Afterwards, the gradient wind speed was compared to the mean wind profiles observed by the Doppler SODAR and by the boundary layer wind-profiler. From the comparisons, the mean wind characteristics and their radial variations in the inland TCBL were studied. In detail, (a) the gradient balance assumption was evaluated using the mean upper-level wind speed calculated by averaging wind speed measurements taken between 1250 m and 1750 m, (b) the super-gradient feature was systematically investigated when the ratios between the observed maximum wind speeds below 1500 m and the calculated gradient wind speeds were plotted against the raw and the normalized radius.

Following this Introduction, Section 2 presents a description of the field measurement (mean wind profile) and the numerical simulation (sea level pressure) data, together with the post-processing procedures to yield both the mean wind profile and the gradient wind speed. Since it is necessary to validate the sea level pressures simulated by a numerical model before the calculation of the gradient wind speed, a validation based on aircraft observations is also described in Section 2. Section 3 discusses the comparison results in terms of the gradient balance assumption and the super-gradient feature. Conclusions are presented in Section 4.

2. Data and post-processing

In Hong Kong, the Hong Kong Observatory (HKO) has setup over forty automated stations all over the territory to monitor wind speeds and directions, in which several stations are equipped with Doppler SODARs and boundary layer wind-profilers, which are capable of measuring wind speeds and directions at various heights up to 5000 m. Using the wind measurements taken during the passages of four typhoons, the vertical profiles of mean wind speeds in the inland TCBL were calculated. The sea level pressure data produced by a numerical model was utilized to calculate the gradient wind speed at the measurement site. In order to validate the use of the sea level pressure data from a numerical model in the calculation of the gradient wind speed, the pressure measurements taken by an aircraft were employed and a sensitivity analysis was conducted.

2.1 Field measurements

While the Doppler SODAR, which stands for Sound Detecting Air Ranging, uses the sound waves to probe the air parcel motion at comparatively low altitudes ($< 200\ m$), the boundary layer wind-profiler, which essentially is the meteorological RADAR, transmits radio waves to higher

altitudes (up to 8 km) and measures the backscattered energy to determine the wind speed and direction at corresponding altitudes. Based on the Doppler Effect, both the DOSAR and the boundary layer wind-profiler measure the air parcel motion in the direction pointed at by the antenna. As both the SODAR and the boundary layer wind-profiler have multiple antennas, which probe the air parcel motions simultaneously, the wind velocity vector is resolved based on the information provided by all the antennas. More specifically, while one antenna points to the zenith to measure the vertical wind speed, others are inclined to the zenith by some degrees to allow the horizontal wind speed to be measured. Both the Doppler SODAR and the boundary-layer wind-profiler calculate the wind speed according to the statistics, mainly the spectra, of the backscattered signals, and the calculated wind speed is therefore a temporal and spatial mean value. As a result, it is usually not necessary to average the raw measurements taken by the Doppler SODAR and the boundary layer wind-profiler to have the mean wind profile. The reliability and accuracy of the Doppler SODAR's and boundary layer wind-profiler's measurements have been substantiated by the work of a number of scholars. For example, Thomas and Vogt (1993) have been operating four different Doppler SODAR systems on a routine basis for more than 10 years, and have compared the resolved wind velocities to the wind measurements taken by conventional meteorological instruments mounted on a 200 m high tower nearby. Similarly, Chan (2008) used the Doppler SODAR measurements to calculate turbulence characteristics and compared the results to the measurements taken by conventional techniques at the same site. Their comparisons showed that the wind measurements taken by the Doppler SODAR are as reliable and accurate as the measurements taken by conventional techniques. For the boundary layer wind-profiler, Heo *et al*. (2003) compared the wind velocities measured by the boundary layer wind-profiler and by the radiosondes launched at the same site, and showed that the measurements taken by the boundary layer wind-profiler share the same credibility as the radiosonde measurements.

For the present study, the wind measurements taken at the Sui Ho Wan (SHW) station were employed to calculate the vertical profiles of the mean wind speeds in the TCBL over land. The geographic location of the SHW station (22°18′21" Latitude and 113°58′45" Longitude) is shown in Fig. 1. The SHW station is located on the northern coast (about 100 m from the coast line) of Lantau Island, which is an island on the western part of the territory of Hong Kong. It can be considered as under marine exposure for the winds coming from the NNE-N-NW directions. Towards the west of the SHW station, there is a piece of flat land (the Hong Kong International Airport) surrounded by open waters. In other directions from the SHW station, i.e., E-SE-S-SW, Lantau Island has some tall mountains, e.g., the Lantau Peak (918 m) to the southwest and the Tai Tung Shan (869 m) to the south.

Both Doppler SODAR and boundary layer wind-profiler equipment were installed in the SHW station, which is 22 m above mean sea level. The Doppler SODAR uses acoustic waves of 4500 kHz to probe the atmospheric boundary layer up to the height of 100 m. Although it takes the Doppler SODAR 1.5 seconds to do a full scan for all three antennas, which means the raw Doppler SODAR measurement corresponds to the 1s gust measurements taken by anemometers, the data available for our study was only 5−min mean wind speeds (provided directly by the HKO), which were calculated by simply averaging the raw Doppler SDOAR measurements. Similarly, although the raw boundary layer wind-profiler measurement corresponds to the 1−min mean wind speed, the raw data was not available and the 10−min mean wind speed calculated by averaging the raw boundary layer wind-profiler measurements was employed. While the height resolution for the Doppler SODAR measurements was 5 m, the height resolution for the boundary layer wind-profiler varies from 60 m for the low-mode to 200 m for the high-mode.

Fig. 1 The geographic location of SHW station

Due to the noisy sound environment near the ground, the measurements taken by the Doppler SODAR at the two lowest heights (5 m and 10 m) were discarded. Since the Doppler SODAR measures wind speeds and directions up to heights of 100 m and the height range of the boundary layer wind-profiler's measurements starts from 113 m, the vertical profile of the mean wind speeds with a time scale equal to 10 minutes can be calculated in two steps. One, the two measurements taken by the Doppler SODAR ($5-\min$ mean) within the $10-\min$ time slot of the boundary layer wind-profiler's measurements were averaged. Two, the averaged Doppler SODAR ($< 100\ m$) and the $10-\min$ mean boundary layer wind-profiler ($> 100\ m$) measurements were then combined to yield the vertical profile of the mean wind speeds up to a height of 5000 m.

Due to the availability of the measurement data, only four typhoon cases were investigated, and only the measurements taken under the influence of the investigated typhoons were employed. Specifically, Typhoon Fengshen (2008), Typhoon Hagupit (2008), Typhoon Nuri (2008) and Typhoon Molave (2009) were investigated. The start and end times defining the investigation period for each typhoon were selected according to the tropical cyclone report prepared by the HKO*. The tracks of the four typhoons investigated are shown in Fig. 2 to indicate how close each typhoon was to Hong Kong. Since the mean wind profiles were compared to the gradient wind speed, which was calculated based on the sea level pressure data outputted by a numerical model, a series of 10 minutes temporal windows inside the investigation period of each typhoon were selected according to the availability of the sea level pressure data. Only the measurements taken inside the windows were employed to calculate the mean wind profiles. For a given sea level pressure field, three temporal windows were selected. While the center of the first window was

* http://www.hko.gov.hk/informtc/tcReporte.htm

specified as the moment at which the sea level pressure field became available, the centres of the second and the third time windows were specified by shifting the first window center by 10 minutes forwards and backwards respectively. For example, the sea level pressure field at 20:00 on 2008-6-23 was made available by the numerical model, and three time slots, i.e., 19:45~19:55, 19:55~20:05 and 20:05~20:10 on 2008-6-23 were selected as the corresponding temporal windows to calculate the mean wind profile. Given the time resolution of the numerical model outputs (3 hours), the sea-level pressure data calculated by interpolation is considered unreliable in the middle between two model outputs. As a result, the measurements taken outsides the temporal windows specified above were not included in the present study. While the gradient wind speed corresponding to the first temporal wind was calculated directly based on the model outputted sea level pressure field, a linearly interpolated field was used to calculate the gradient wind speed corresponding to the second and the third temporal windows. Since the second and third temporal windows are close to the sea level pressure field output moment, the linear interpolation results should be considered reliable.

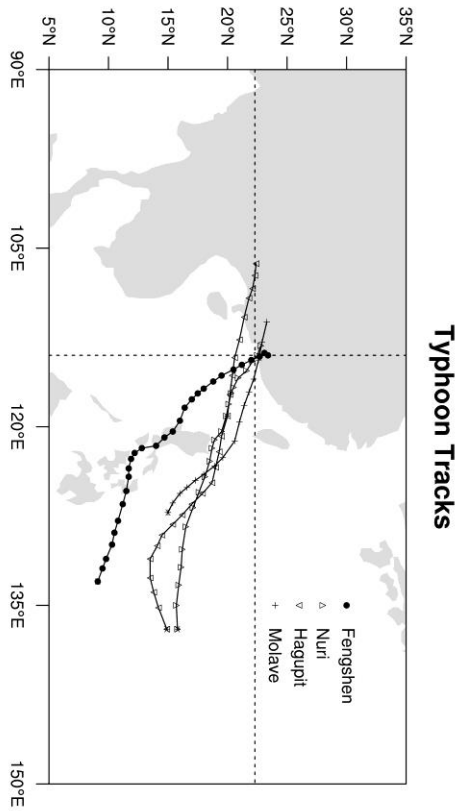

Fig. 2 The tracks of the four typhoons under investigation, each knot in their track shows the location of the storm center at a time interval of 6 hours. The starting time for the four typhoons are 2008-6-12 12:00 (Fengshen), 2008-8-17 12:00 (Nuri), 2008-9-19 0:00 (Hagupit) and 2009-7-15 12:00 (Moalve). The location of the SHW station is indicated by the cross of two dashed lines

2.2 Sea-level pressure

The Operational Regional Spectral Model (ORSM)[†], which is utilized by the HKO to routinely run weather forecasts for Hong Kong, was used to do the simulation for the investigation periods defined in calculating the mean wind profiles (subsection 2.1). From the numerical simulation results, the sea level pressure data was extracted. Since the observations obtained from foreign sources and from the local network were ingested into ORSM through a 4D-VAR approach (JMA 2002), the reliability and accuracy of the model outputs are better than stand-alone numerical weather predictions (Yeung *et al*. 2005). In the ORSM, two simulation domains are nested. While the smaller domain, with the horizontal spacing of 20 km, covers Hong Kong and its neighbouring areas, the larger domain, with horizontal spacing of 60 km, covers East Asia and the West Pacific. The vertical discretization (40 layer) is the same for both domains, and the higher resolutions are found near the surface. The temporal resolution of the outputs from the nested domain, whose results were utilized in the present study, was 3 hours. While the model output from the last cycle ingests the real-time observations to provide the initial condition for the current cycle (the so-called "warm start"), the lateral boundary condition is extracted from the output of a global model (Japanese Meteorology Agency's global spectral model[‡]).

Using the sea level pressure data provided by the ORSM, the gradient wind speed at the SHW station was calculated using a tropical cyclone pressure-wind model. In detail, it is conventionally acceptable that the sea level pressure in a tropical cyclone weather system can be modelled as,

$$\mathrm{p(r)} = p_c + \Delta p \exp\left[-\left(\frac{r_{max}}{r}\right)^b\right] \tag{1}$$

In Eq. (1), $\mathrm{p(r)}$ is the pressure at radius r, p_c is pressure at the center of a tropical cyclone, $\Delta\mathrm{p}$ is the difference between the central pressure and the ambient pressure (central pressure drop), r_{max} is the RMW and b is a model parameter determining the shape of the horizontal pressure profile. Using the two dimensional Nelder-Mead simplex algorithm, the sea level pressure data provided by the ORSM was fitted to Eq. (1). From the fitting results, the location of the tropical cyclone center and the model parameters in Eq. (1) (p_c,r_{max},b) were obtained. Through applying the gradient balance assumption to the radial profile of the sea level pressure described by Eq. (1), Holland (1980) derived a radial profile of the gradient wind speed as

$$\mathrm{V(r)} = \sqrt{\frac{{r_{max}}^b b\Delta p \exp\left[-\left(\frac{r_{max}}{r}\right)^b\right]}{\rho r^b} + \frac{r^2 f^2}{4}} - \frac{rf}{2} \tag{2}$$

In Eq. (2), $\mathrm{V(r)}$ is the radial profile of the gradient wind speed, ρ is the air density near the sea surface and takes the value of $1.15\ \mathrm{kg/m^3}$ following the suggestion by Holland (1980) and f is the Coriolis parameter. As the locations of the tropical cyclone centers and the SHW station are expressed in terms of the longitudes and latitudes, the Lambert Conformal Conic map projection was employed to calculate the distance from the storm center to the SHW station (r in Eqs. (1) and (2)). To define a Lambert Conformal Conic map projection, the two "true latitudes" were specified as $10°\mathrm{N}$ and $30°\mathrm{N}$ and the center of the projection was specified as $115°\mathrm{E}$ and $20°\mathrm{N}$. Based on the distance from the storm center to the SHW station, the model parameters ($\Delta\mathrm{p}, r_{max}, b$)

[†] http://www.hko.gov.hk/wservice/tsheet/nwp.htm
[‡] http://www.jma.go.jp/jma/en/Activities/nwp.html

derived from the fitting process and the Coriolis parameter (f) corresponding to the latitude of the SHW station, the gradient wind speed at the SHW station was calculated.

2.3 Data post-processing

Since measurement errors were inevitable, especially when the boundary layer wind-profiler and the Doppler SODAR are employed to take measurements under the influence of complex weather processes, it is necessary to preselect the observed mean wind profiles before comparing with the gradient wind speed calculated from the horizontal variation of the sea level pressure. More specifically, the observed mean wind profile below 200 m was fitted to the log-law model, which derived both the friction velocity u_* and the aerodynamic roughness length z_0. After normalizing the observed mean wind velocity by the friction velocity and the height by the aerodynamic roughness length, the correlation coefficient was calculated using the normalized velocity and the logarithm of the normalized height. The observed mean wind profile would be discarded if the calculated correlation coefficient was less than 0.75. Fig. 3 shows the normalized wind velocities and the normalized heights below 200 m from the profiles included in the comparisons to the gradient wind speed. It is evident that the measurements from the selected profiles are sufficiently close to the log-law model (solid line).

Besides the measurement errors, the two-dimensional fitting process, which yielded parameters to calculate the gradient wind speed, may occasionally lead to unrealistic results. Therefore, it is necessary to quality-check the fitting results before the parameters are used to calculate the gradient wind speed. The quality-check consisted three components: (a) the storm locations (the longitudes and the latitudes) was checked in terms of continuity, (b) the model parameters (Δp, r_{max}) were checked to ensure their values were in reasonable ranges ($10\ \text{mb} < \Delta p < 100\ \text{mb}$, $20\ \text{km} < r_{max} < 200\ \text{km}$), and (c) the comparison between the sea level pressure data simulated by the ORSM and the calculation results of Eq. (1) was checked to ensure that Eq. (1) adequately describes the radial variations of the sea level pressure. In other words, the root mean squared difference between the simulated (from ORSM) and the calculated (from Eq. (1)) sea level pressures was checked to ensure it is smaller enough ($< 1.5\ \text{mb}$) for the parameters (Δp, r_{max} and b) to accurately represent the characteristics of the sea level pressure data provided by the ORSM.

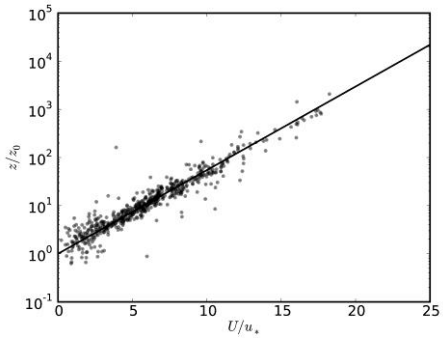

Fig. 3 The measurements below 200 m selected for the present study. While the wind velocity is normalized by the friction velocity u_*, the height is normalized by the aerodynamic roughness length z_0. The solid line shows the log-law calculation

Table 1 The investigation moments and some fitting results

Time	Pressure drop (mb)	RMW (km)	R.M.S.D.[i] (mb)	Sensitivity (%)
2008-06-23_17:00	33.80	104.209	0.6135	0.22
2008-06-23_20:00	30.99	121.946	0.4404	0.09
2008-06-24_02:00	31.47	100.932	1.1164	0.56
2008-06-24_05:00	35.39	108.403	0.7867	0.42
2008-06-24_17:00	33.19	96.998	0.2683	0.03
2008-06-24_20:00	33.68	89.875	0.9227	0.67
2008-06-24_23:00	23.61	123.747	0.6994	1.79
2008-06-25_02:00	25.55	116.503	1.0383	1.74
2008-06-25_05:00	25.80	125.559	0.8431	2.24
2008-06-25_14:00	23.26	95.387	0.2493	0.49
2008-06-25_17:00	24.27	63.388	0.2398	2.95
2008-08-21_17:00	43	65.363	0.4022	0.40
2008-08-21_20:00	41.87	90.907	0.3051	0.31
2008-08-21_23:00	40.65	105.205	0.9264	0.31
2008-08-22_02:00	40.13	100.173	0.5107	0.51
2008-08-22_11:00	35.88	82.584	0.4042	0.95
2008-08-22_17:00	32.49	114.253	1.1882	1.18
2008-08-23_02:00	26.41	71.046	0.2710	1.23
2008-08-23_05:00	17.49	172.488	0.2521	0.13
2008-09-23_02:00	57.29	94.065	0.3403	0.39
2008-09-23_05:00	62.59	91.716	0.3898	0.39
2008-09-23_08:00	65.55	72.509	0.4300	0.43
2008-09-23_17:00	66.41	71.633	0.5721	0.59
2009-07-18_11:00	40.89	84.144	0.1042	0.10
2009-07-18_17:00	43.7	79.579	0.1974	0.21
2009-07-18_23:00	39.15	67.885	0.9418	0.32
2009-07-19_02:00	42.4	53.498	0.8736	0.87
2009-07-19_05:00	33.86	92.164	0.4396	1.92
2009-07-19_11:00	22.91	165.916	0.8022	0.16

[*] R.M.S.D. stands for the root mean squared difference

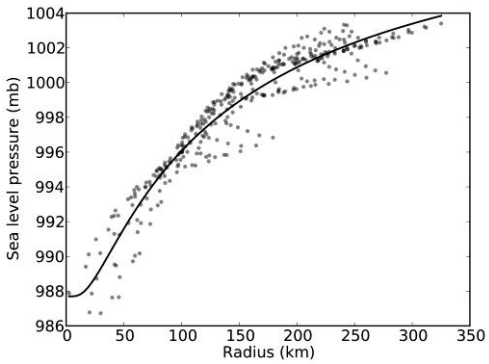

Fig. 4 The sea level pressures at 2008-6-25 02:00 provided by the ORSM (dots) and the two dimensional fitting result (solid line) calculated from Eq. (1). The root mean squared difference for the comparison is 1.038 mb

After the quality check, only a few sea level pressure fitting results remained for the calculation of the gradient wind speed. Table 1 summarizes the model parameter derived from the fitting process. In order to illustrate the criterion (c) in the quality-check of the sea level pressure fitting results, the fitting results corresponding to the time 2008-6-25 02:00 are used as an example. Fig. 4 presents the comparison between the scatter of the sea level pressures provided by the ORSM and the radial profile calculated according to Eq. (1) using the parameters derived from the fitting. Since the root mean squared difference for the comparison shown in Fig. 4 is 1.038 mb and the maximum root mean square difference shown in Table 1 is 1.188 mb, the model parameters contained in Table 1 should be considered as adequately describing the characteristics of the sea level pressure data provided by the ORSM.

2.4 Validation for ORSM and the sensitivity analysis

Since the gradient wind speed calculated based on the sea level pressure data provided by the ORSM is the key component in an investigation on both the gradient balance assumption and the super-gradient feature, it is necessary to validate the outputs from the ORSM before the parameters derived from the fitting process are used to calculate the gradient wind speed. It is obvious that a thorough and comprehensive validation is extremely difficult, if not impossible, and beyond the scope of the present study. Specifically, the comprehensive validation requires dense observations of various meteorology variables covering the entire domain of the ORSM model. Provided that the purpose of the validation is merely to assess the reliability of the sea level pressure data output from the ORSM, it is adequate to only compare the observations obtained by research aircraft in several flight legs to the field simulated by the ORSM. A research aircraft was used by the HKO from time to time to probe the wind shear and turbulence in the atmospheric boundary layer near the Hong Kong International Airport, and air pressure measurements taken by the research aircraft in the vicinity of Typhoon Molave (2009) were employed to estimate the sea level pressure underneath the flight leg. The estimated sea level pressures were then compared to the sea level pressures simulated by the ORSM at the same locations, and the mean difference between estimated and simulated sea level pressures were employed to indicate the reliability of the ORSM

outputs.

In mid-2009, an Aircraft Integrated Meteorological Measuring System was installed on one of the fixed-wing aircraft owned by the Government Flying Service of the Hong Kong Government to take in-situ meteorological measurement over the South China Sea (Chan *et al*. 2011). Due to the sparseness of the meteorological measurements collected over the South China Sea, the information provided by the research aircraft is valuable in terms of investigating the TCBL. On the afternoon of July 18th, 2009, the research aircraft was sent out for a rescue mission. During the mission, the aircraft continuously took measurements of altitudes, pressures, temperatures, horizontal wind speeds and relative humidity. The measurements were taken at a frequency of 20 Hz, and the resolution of the pressure measurements, which is the only measurement employed in the present study, was 0.1 mb. For the mission on July 18th, 2009, the aircraft flew for more than 4 hours and approached the center of Typhoon Molave (2008) from the north and the north-northwest. During 09:40 ~ 10:00, the aircraft was closest to the storm center (~90 km). For the rest of the mission, the aircraft kept a distance of ~ 100 km or larger from the storm center. The flight altitude was comparatively low when the aircraft patrolled in a search mode (in the range of 200 mm ~ 700 m).

Using the air pressure and height measurements taken during the patrol, the sea level pressures underneath the flight leg were estimated by the hydrostatic relationship. More specifically, the sea level pressure was estimated based on the flight level pressure as

$$\mathrm{p}_0 = p\left(1 - \frac{LH}{T+LH}\right)^{-\left(\frac{gM}{RL}\right)} \tag{3}$$

In Eq. (3), p_0 is the sea level pressure, p is the pressure at the flight level, L is the lapse rate and takes the value of 0.0065 K/m, H is the height of the aircraft from the sea surface, T is the air temperature measured at the flight level, g is the gravity (9.81 m/s^2), M is the molar mass of the air (0.02896 kg/mol) and R is the universal gas constant (8.3144 J/(mol · K)). Although the hydrostatic assumption, based on which Eq. (3) is derived, is only valid in an approximate sense, it is acceptable to use Eq. (3) to estimate the sea level pressure given that the height of the research flight was sufficiently low (Smith 1968, Smith and Montgomery 2008).

Figs 5(a) and 6(a) show two flight legs, on top of the contours of the sea level pressure provided by the ORSM, extracted from the flight mission on July 18th, 2009. It is obvious that in both flight legs, the research aircraft approached the center of the storm and turned back. Therefore, it is expected that the air pressure measurements taken by the aircraft show an identifiable variation (increase after decrease) to compare to the sea level pressure output from the ORSM. Given the longitudes and latitudes, which were measured by the aircraft in real-time, the sea level pressure underneath the flight legs shown in Figs. 5(a) and 6(a) can be calculated by spatially interpolating from the sea level pressure simulated by the ORSM. Furthermore, a temporal interpolation was conducted, on top of the spatial interpolation, to calculate the sea level pressure at the moments reported by the aircraft from two sea level pressure fields consecutively outputted from the ORSM. Figs. 5(b) and 6(b) show the comparisons between the sea level pressures estimated from the aircraft measurements and simulated by the ORSM. It is apparent that the simulated pressure is in acceptable agreement with the estimations based on the aircraft measurements. In fact, the mean deviations, from the numerically simulated values to the estimations, were 0.56 mb and 0.89 mb respectively for flight legs shown in Figs. 5 and 6.

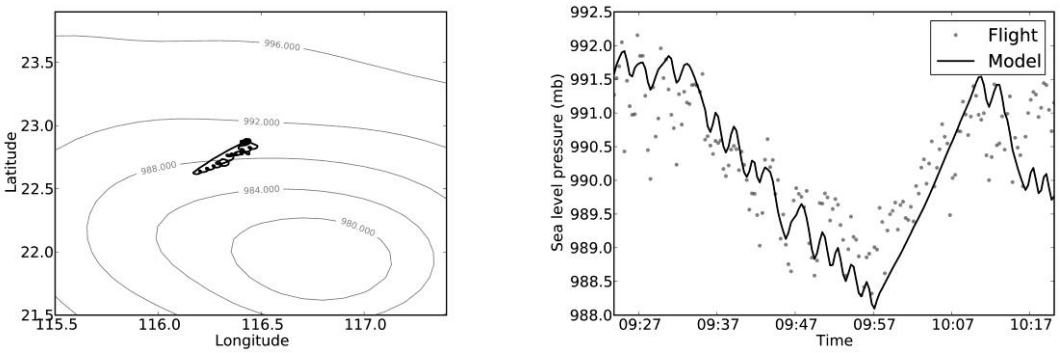

(a) Flight leg pattern (b) Pressure variation

Fig. 5 The flight pattern on top of the sea level pressure contour (a) and the comparison between the sea level pressures simulated by ORSM and estimated based on aircraft observations. The aircraft measurements were taken during 09:25 ~ 10:20 on 2009-7-18

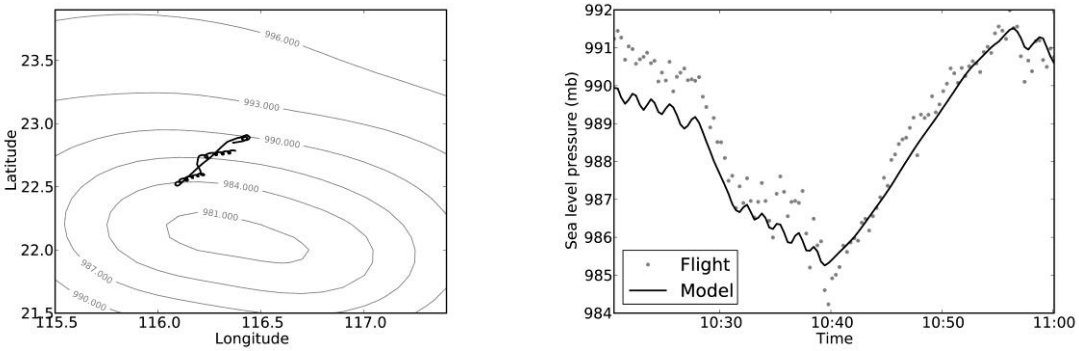

(a) Flight leg pattern (b) Pressure variation

Fig. 6 The flight pattern on top of the sea level pressure contour (a) and the comparison between the sea level pressures simulated by ORSM and estimated based on aircraft observations. The aircraft measurements were taken during 10:21 ~ 11:00 on 2009-7-18

More importantly, Figs. 5(b) and 6(b) show that the variation of the sea level pressure simulated by the ORSM underneath the flight legs match with the variations observed by the aircraft. Theoretically, the gradient wind speed should be calculated using the horizontal pressure variations at the same vertical level, and hence the gradient wind speed calculated using the sea level pressure data only shows the gradient wind strength at the sea surface. As a result, it is not applicable to compare the gradient wind speed calculated from the sea level pressure data to the observed wind speed at higher level (~1000 m). The vertical variation of the horizontal pressure gradients is, however, found to be negligibly small in the TCBL (Smith 1968, Smith and Montgomery 2008). In other words, Smith (1968) and Smith and Montgomery (2008) indicated that the gradient wind speed calculated using the sea level pressure data approximately equals the gradient wind speed calculated using the horizontal pressure field inside or just above the TCBL. Their conclusions were partially substantiated by the comparison shown in Figs. 5(b) and 6(b) as

the horizontal variations of the pressure measured at the flight level are similar to the sea level pressure simulated by the ORSM. As a result, it is practically acceptable to compare the gradient wind speed calculated based on the sea level pressure data to the observed mean wind speed within or just above the TCBL. From another perspective, the work of Powell *et al*. (2009) showed that the RMW at the sea level is on average 0.875 of the RMW at the flight level (~3 km). Based on a simple linear interpolation, the RMW at the level just above the TCBL (~1 km) can be estimated as 1.048 times the RMW at the sea level. Using the model parameters shown in Table 1, the relative difference of 0.048 in the RMW would result differences in the calculated gradient wind speed not exceeding 0.6 m/s, or 4% when normalized by the gradient wind speed calculated using the original sea level pressure data. In other words, the error induced by calculating the gradient wind speed at a level of 1000 m using the sea level pressure data is negligible given that the estimate by Powell *et al*. (2009) is reliable.

Although the comparisons shown in Figs. 5 and 6 and the discussion presented above preliminarily show the validity of using the ORSM simulated sea level pressure data to calculate the gradient wind speed, the calculated gradient wind speed was not directly compared to the observations, and hence the uncertainty associated with the gradient wind calculations is still unclear. In order to assess the reliability of the calculated gradient wind speed at the SHW station, the ORSM outputted sea level pressure field was perturbed by a random field constituted by a grid of normally distributed random variables with zero means. When the standard deviations of the normally distributed random variable varied from 0 mb to 2.5 mb, the influence of the perturbations, with magnitudes similar to the mean deviations shown in Figs. 5(b) and 6(b), on the calculation of the gradient wind speed was investigated. Fig. 7 shows the relative difference in the calculation of the gradient wind speed at the SHW station induced by the perturbation in the sea level pressure data. The relative difference is defined as the absolute difference between the gradient wind speeds calculated based on the perturbed and unperturbed sea level pressure fields normalized by the unperturbed gradient wind speed. The two sea level pressure fields (corresponding to 08:00 and 11:00 on 2009-7-18) involved in calculating the curves shown in Figs. 5(b) and 6(b) were employed to calculate the difference shown in Fig. 7. It is seen from Fig. 7 that the perturbation with magnitude, which is defined as the standard deviation of the normally distributed random variable, of 1 mb means a deviation of $< 2\%$ in the gradient wind speed calculation for the two sea level pressure fields under investigation. Given that the mean deviation of the numerically simulated sea level pressure from the estimations based on the aircraft observations are less than 1 mb (Figs. 5(b) and 6(b)), perturbations with magnitude of 1 mb were added to all the sea level pressure fields included in the present study to assess the risibilities of the gradient wind speeds comparing with the observed mean wind profiles. The resulting relative difference was always less than 3% (a maximum value of 2.95%) and most of the relative differences were less than 1%. In order to better show the reliability of the calculated gradient wind speed, the relative differences resulting from the perturbation with a magnitude of 1 mb for all the sea level pressure fields contained in Table 1 were calculated and are summarized in the last column of Table 1.

In summary, the comparison between the sea level pressures estimated based on the aircraft measurements and simulated by the ORSM indicates that the sea level pressure field provided by the ORSM is reliable in terms of calculating the gradient wind speed. Furthermore, a sensitivity analysis has shown that the calculation of the gradient wind speed at the SHW station is not sensitive to the perturbations in the sea level pressure field, having the magnitude similar to the

deviation of the ORSM simulated sea level pressures from the estimations based on the aircraft measurements.

3. Discussion

Comparing the mean wind profiles observed at the SHW station to the gradient wind speed calculalted based on the seal level pressure data provides some insights into the mean wind charactersitics in the TCBL over land. The discussion based on the comparison results includes, (a) an evaluation of the gradient balance assumption and (b) an investigation on the super-gradient feature.

3.1 Gradient balance

As pointed out by Willoughby (1990), the wind speeds above the TCBL are required to be in the gradient balance for the simple vortex model to explain convective ring contractions. In addition, the TCBL wind field model developed by Kepert (2001) assumes that the wind speed at a sufficiently high altitude is in the gradient balance. Due to the importance of the gradient balance assumption in tropical cyclone wind field modelling, it has been intensively investigated by previous scholars using mainly the measurements taken over open waters. In the present paper, the wind measurements taken over land were compared to the calculated gradient wind speed to explore the validity of the gradient balance assumption in the tropical cyclone wind field over land. In detail, the wind measurements taken between 1250 m and 1750 m were averaged to calculate the mean upper-level wind speed, which was then compared to the gradient wind speed calculated based on the sea level pressure data. In order to systematically show the validity of the gradient balance assumption, the ratios between the observed mean upper-level wind speeds and the calculated gradient wind speeds were plotted against the raw and the normalized radius. The normalized radius is essentially a ratio between the actual distance from the storm center to the SHW station and the RMW.

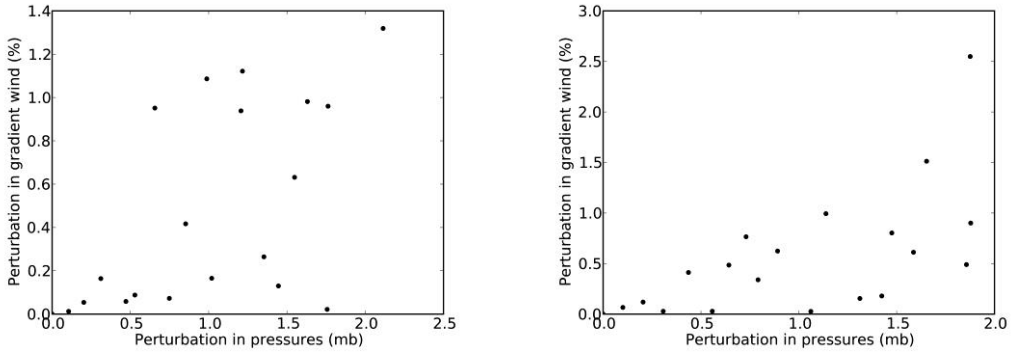

(a) 2009-7-18 08:00 (b) 2009-7-18 11:00

Fig. 7 The variations of the calculated gradient wind speed at the SHW station (following equation (2)) with the perturbations in the sea level pressure data. The subfigure title indicate the time stamp of the sea level pressure data

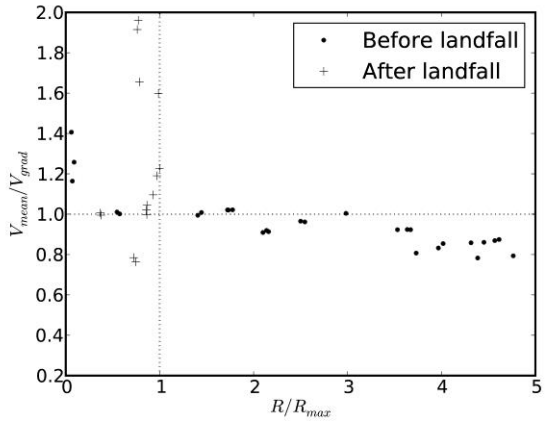

Fig. 8 The radial variation, with the normalized radius, of the velocity ratio between the observed upper-level mean wind speed and the calculated gradient wind speed

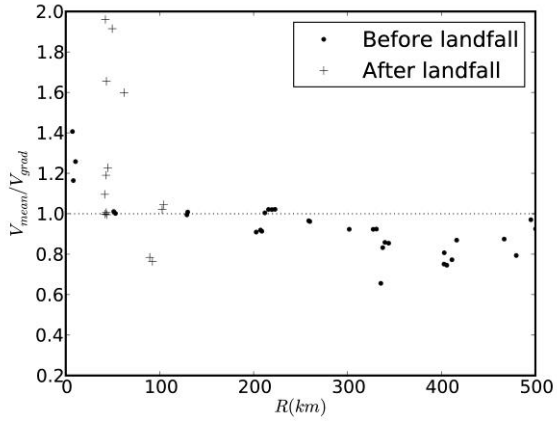

Fig. 9 The radial variation, with the raw radius, of the velocity ratio between the observed upper-level mean wind speed and the calculated gradient wind speed

Fig. 8 shows the radial variation of the ratio with the normalized radius. It is evident that the gradient balance is a valid assumption to describe the inland wind field in tropical cyclones when the normalized radius ranges from 1 to 3. Since the wind speed above the TCBL is not directly influenced by the underlying terrain, the upper-level mean wind speed is expected to follow the law discovered through analysing the wind speed variations in tropical cyclones over open waters, i.e. the gradient balance relationship. When the normalized radius exceeds 3, the observed upper-level mean wind speed was found to be apparently less than the gradient wind speed calculated by fitting the sea level pressure data to Eq. (1). Such an observation does not indicate the failure of the gradient balance assumption, rather, it implies the deficiency of Eq. (2) when it is used to calculate the gradient wind far away from the storm center (normalized radius larger than

3). It is obvious that Eq. (2) is only applicable when the calculation is for a site under the influence of tropical cyclone meteorology. In the region far away from the storm center, it is not reasonable to expect Eq. (2) to reliably calculate the gradient wind speed as the region might be dominated by other weather processes. As shown in Fig. 8, the calculation according to Eq. (2) tends to overestimate the upper-level mean wind speed in the region far away from the storm center. It, however, might not be the case when the region is dominated by other severe weather process.

For the upper-level wind speeds inside the RMW, Fig. 8 indicates that the gradient balance is not applicable, and the observed mean upper-level wind speed is found to be obviously larger than the calculated gradient wind speed. This finding contradicts the conclusion reached by Gray (1991), which stated that, "the inner core of a tropical cyclone must be close to the gradient balance". When the ratios corresponding to the observations obtained after the landfall were separated from those corresponding to observations obtained before the landfall (as shown in Fig. 8), it can be observed that landfalls have an appreciable impact on how the observed upper-level mean wind speed is compared to the calculated gradient wind speed inside the RMW. In fact, except when the normalized radius is extremely small (< 0.1), the ratios indicating that the calculated gradient wind speed underestimates the upper-level wind speed all belong to the after landfall category. Since the TCBL dynamics over land, which are crucial in shaping the overall tropical cyclone wind field, are certainly different from the TCBL dynamics over open waters, it is speculated that the presence of a large piece of land beneath the TCBL wind field is responsible for the super-gradient state of the upper-level wind observed inside the RMW in Fig. 8. More specifically, it is argued that the pressure field in the tropical cyclone atmosphere is more sensitive to the change in the underlying boundary condition than the horizontal wind field. When the pressure field is modified by the presence of a large piece of land, the cyclonic rotation still brings winds full of momentum from the wind field over open waters to influence an island site, such as the SHW station. The mechanism is explored in more detail in the investigation of the super-gradient flow inside the TCBL (subsection 3.2).

In order to show the effect of the tropical cyclone size, the ratio between the observed upper-level mean wind speed and the calculated gradient wind speed is also plotted against the actual radius from the tropical cyclone center to the SHW station (Fig. 9). Similar features, as in Fig. 8, can be observed in Fig. 9. Specifically, the upper-level mean wind speed is found to be close to the calculated gradient wind speed when the radius is in the range of 120 km ~ 250 km. When excluding the ratios belonging to the after landfall category, the validity of the gradient balance assumption can be extended inward to a radius of 50 km, as shown in Fig. 9.

3.2 Super-gradient flow

As a distinctive feature of the TCBL wind field, the wind maxima in the TCBL are frequently found to be larger than the gradient wind speed in the lower troposphere, which indicates that the wind flow in the TCBL is super-gradient. It is well established, from both the theoretical perspective and observational perspective, that super-gradient flow is present in the TCBL over open waters. Although the low-level wind maxima were also found from the wind profiles observed by the inland radars when tropical cyclones were approaching (Giammanco *et al*. 2013), the vertical variation of the mean wind speed over land is not as systematic as over open waters. In fact, it has been found that the profile model introduced by Vickery *et al*. (2009) is not applicable for describing the mean wind profile in the TCBL over land (Tse *et al*. 2013). As a result, the investigation on the super-gradient feature for the TCBL wind field over land should be

independent from the model of Vickery *et al*. (2009) and should not focus on the well-defined low-level peaks in the wind profile. In the present paper, the ratio between the observed maximum wind velocity below 1500 m and the calculated gradient wind speed were plotted against the raw and the normalized radius to show the presence of the super-gradient flow in the TCBL.

It is clear from Fig. 10, which shows the radial variation of the ratio with the normalized radius, that the super-gradient flow was mainly observed slightly inwards from twice the RMW. In fact, all the observations imply the existence of the super-gradient flow when the normalized radius is less than 1.6. In addition, the ratio increases, in general, with the decreasing normalized radius. In other words, the super-gradient flow in the TCBL becomes more and more obvious when moving towards the storm center. While the study of Giammanco *et al*. (2013) concluded that the wind profiles measured over land with low-level peaks was typically found at, or inside, the RMW of a tropical cyclone, Fig. 10 indicates that the super-gradient feature could be found in the radial range from the RMW to twice the RMW. For an outside site located outwards twice the RMW, the wind flow in the inland TCBL could be either sub-gradient or super-gradient and the systematic variation is absent. It should be pointed out that, however, the work of Giammanco *et al*. (2013) took the well-defined low-level jet as the presence of the super-gradient flow. In the present study, the super-gradient flow is defined differently as in the comparision with the gradient wind speed calculated based on the sea level pressure data. Therefore, the conclusion on the presence of the super-gradient flow reached through investigating Fig. 10 could be found to be compatible with the findings made by Giammanco *et al*. (2013). In other words, given that the gradient wind speed is calculated based on the horizontal pressure varaition, the super-gradient flow can be found from the mean wind profiles observed inside twice the RMW based on the data collected by Giammanco *et al*. (2013), even through the profile has no well-defined low level jet.

As in the evaluation of the gradient balance assumption, Fig. 11 present the ratios between the maximum wind speed beblow 1500 m and the calculated gradient wind speed varying with the actual radius from the tropical cyclone center to the SHW station. Compared with Figs. 10 and 11 shows that the super-gradient flow is systematically observed inside a radius of 200 km.

In addtion, the increasing trend of the ratio with the decreasing radius is repeated in Fig. 11, which indicate that, regardless of the size of the tropical cyclone, the wind field in the inland TCBL becomes more and more super-gradient when moving towards the tropical cyclone center. Again, Fig. 11 indicates a considerably wider region for the presence of the super-gradient flow in the inland TCBL compared to the value suggested by Giammanco *et al*. (2013) (60 km).

The fact that Giammanco *et al*. (2013) defined the presence of super-gradient flow according to the well-defined low-level peak could be the explanation for the difference, as in the dicussion concerning Fig. 10.

When the observations obtained before the landfall were separated from the observations obtained after the landfall, it is apparent that the wind flow in the inland TCBL is more super-gradient after the landfall. Considering that the mean upper-level wind speeds calculated from the observations obtained after the landfall were also larger than the calculated gradient wind speed inside the RMW (Fig. 8), it is evident that the wind speed calculated based on the sea level pressure data according to Eq. (2) underestimates the overall wind strength inside the RMW after landfall. Since the observed wind speeds are higher than the calculated gradient wind speeds for the majority of the comparisons shown in Figs. 8 and 10, it is very unlikely that the underestimation can be explained by either the measurement error contained in the observed mean wind profile or the inaccurate sea level pressure fitting results. Instead, the underestimation implies the nature of the TCBL wind field over land. In our opinion, the underestimation is due to

the unsynchronized decay of the sea level pressure and the wind strength in a tropical cyclone after the landfall. As stated in the discussion on the gradient balance, it is speculated that the pressure field decays faster than the wind field in the TCBL. In detail, the vertical convection near the tropical cyclone center, which maintains the low pressure in the tropical cyclone center, is significantly reduced due to the absence of surface sensible and latent heat fluxes when a tropical cyclone makes a landfall (Powell 1987). As a result, the pressure field in the TCBL rapidly decays after the landfall. The horizontal wind field, however, maintains the strength after a landfall for a relatively long period as the cyclonic rotation keeps bringing strong winds from the over-water-portion of the tropical cyclone. Therefore, the gradient wind speed calculated based on the sea level pressure field after a landfall underestimates the overall wind strength, regardless of the vertical level (inside or above the TCBL).

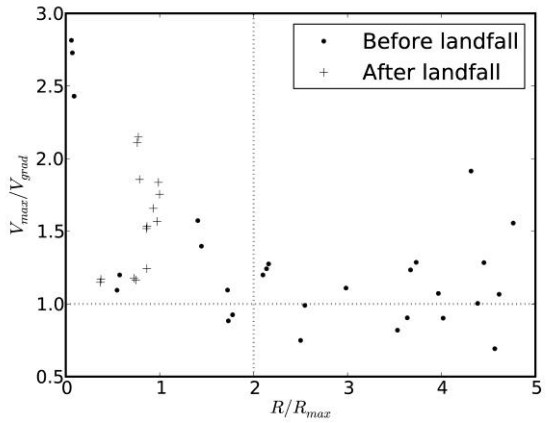

Fig. 10 The radial variation, with the normalized radius, of the velocity ratio between the observed maximum wind speed below 1000 m and the calculated gradient wind speed

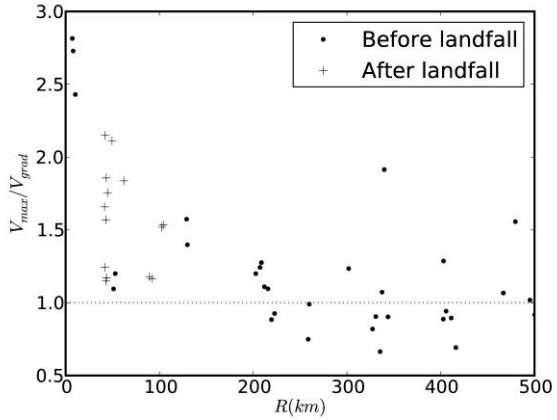

Fig. 11 The radial variation, with the raw radius, of the velocity ratio between the observed maximum wind speed below 1000m and the calculated gradient wind speed

In order to better illustrate the mechanism explaining the super-gradient flow observed after the landfall, Typhoon Fengshen (2008) was investigated as an example. Fig. 12(a) shows the variations of the central pressure drop (Δp in Eq. (1)) and the RMW with time. The moment when the typhoon made landfall is taken as the origin point of the axis (Hour 0). It is obvious that Δp decreases significantly around the Hour 0 (from 33.1 mb to 23.6 mb). Although the RMW is not as sensitive as the central pressure drop, it obviously changes when crossing the Hour 0. In fact, the RMW decreases from 89.9 km (corresponding to the Hour -2) to 62.9 km (corresponding to Hour 16). The decreases in both the central pressure drop and the RMW leads to the decrease of the calculated gradient wind speed at the SHW station, which is shown in Fig. 12(b). The variations of the upper-level mean wind speed and the maximum wind speed below 1500 m are also included in Fig. 12(b). As indicated by the variations of wind speeds, while the calculated gradient wind speed decreases, the maximum wind speed below 1500 m increases. From the explanations presented above, the increase is probably due to the strong winds brought by the cyclonic rotation to the SHW station from the over-open-water part of the tropical cyclone. The wind vector plots shown in Fig. 13 substantiate the explanation. Specifically, the wind velocity measurements taken at Hour -2 and Hour 7 below 1500 m are plotted as vectors in Fig. 13. Considering the surrounding environment of the SHW station shown in Fig. 1, the observed wind directions shown in Fig. 13 indicate that the low wind speed observed at Hour -2.0 is associated with the wind coming from the land while the high wind speed observed at Hour 7.0 is associated with the wind coming from the sea. It should be noted that the mechanism detailed above is only a preliminary try to explain the observations concerning the super-gradient flow observed inside the RMW after the landfall of a tropical cyclone. A father study based on a detailed structure of the inland tropical cyclone atmosphere is therefore necessary to check the validity of the mechanism presented.

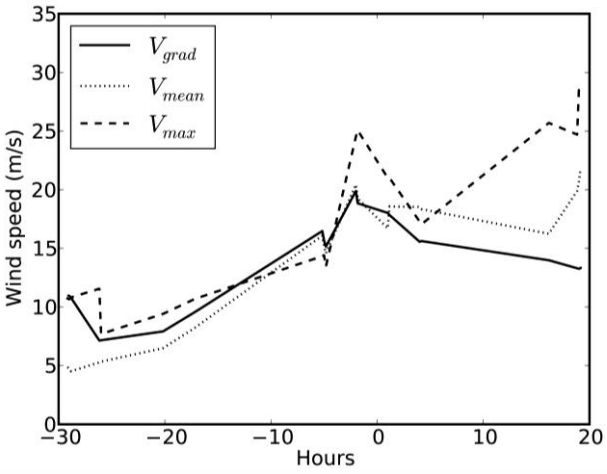

Fig. 12 The variation of the central pressure drop, the RMW, the calculated gradient wind speed and two observed wind speeds (upper-level mean and maximum below 1000 m) with time in Typhoon Fengshen (2008). The Hour 0 was chosen to be the moment the tropical cyclone made a landfall

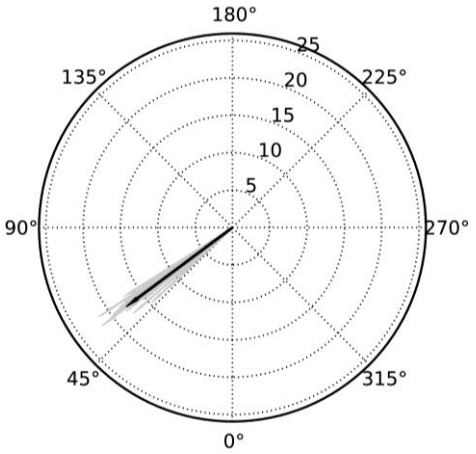

(a) 19:55~20:05 on 2008-6-24

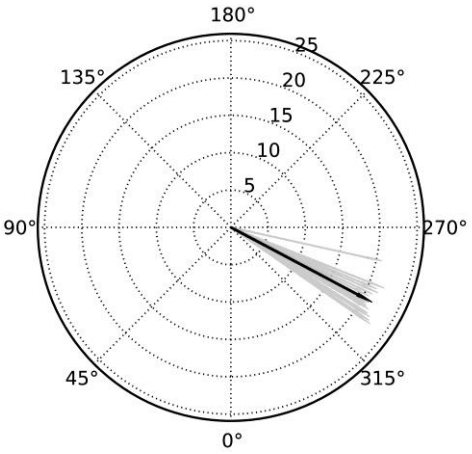

(b) 04:55~05:05 on 2008-6-25

Fig. 13 The vector plots showing the wind directions observed below 1250 m for two periods in Typhoon Fengshen (2008). The bold arrow shows the mean wind velocity vector

4. Conclusions

Using the wind measurements taken by both the Doppler SODAR and the boundary layer wind-profiler at a weather station in Hong Kong during the passages of four typhoons, the vertical profiles of mean wind speeds were calculated. In addition, the sea level pressure data was made available by a numerical model (ORSM). By fitting the sea level pressure data to the model introduced by Holland (1980), the gradient wind speed was calculated for the measurement site. Through comparing the gradient wind speed to the mean upper-level wind speed and the maximum wind below 1500 m, the gradient balance assumption was evaluated and the super-gradient feature was systematically investigated. The upper-level mean wind speed was calculated by averaging the wind speed measurements taken in between 1250 m and 1750 m.

From investigating the variations of the mean upper-level wind speed, the maximum wind speed below 1500 m and the calculated gradient wind speed with the raw and the normalized radius (normalized by the RMW of the tropical cyclone), it has been found that the gradient balance assumption is valid for estimating the upper-level mean wind speed over land outside the RMW and within a distance of three times the RMW. For the upper-level wind speed inside the RMW, the calculated gradient wind speed underestimates the overall wind strength, especially after the tropical cyclone has made landfall.

For the super-gradient feature in the TCBL, it has been found that the wind flow below 1500 m inside twice the RMW is mainly super-gradient. As in the case of the upper-level mean wind speed, the inland TCBL wind field was found more super-gradient after the landfall. In other words, the gradient wind speed calculated using the large-scale sea level pressure data underestimates the overall wind strength inside the RMW after the landfall. It is argued that the unsynchronized decay of the pressure field and the wind field in the TCBL is the reason for such an observation. When a tropical cyclone makes a landfall, the decayed vertical convection leads to a rapid reduction of the central pressure drop. The horizontal wind field is, however, not as sensitive as the pressure field to the vertical convection near the tropical cyclone core, and the wind strength at an island site can be maintained, or even enhanced, by the cyclonic rotation bringing strong winds from the over-open-water part of the tropical cyclone. Although evidence was found to preliminarily substantiate the mechanism presented above, it requires further study, in which the detailed structures of the pressure and wind fields in the TCBL are examined, to confirm its validity.

Acknowledgements

The study reported in this paper was carried out under the support of the RGC General Research Fund, HKSAR Project No. 9041338 for which the authors would like to express their gratitude.

The authors also like to thank the support of the Hong Kong Observatory to this joint research project and for the permission to use the wind data for this research.

References

Chan, P.W. (2008), "Measurement of turbulence intensity profile by a mini-sodar", *Meteorol. Appl*., **15**(2), 249-258.

Chan, P.W., Hon, K.K. and Foster, S. (2011), "Wind data collected by a fixed-wing aircraft in the vicinity of a tropical cyclone over the south China coastal waters", *Meteorol. Z*., **20**(3), 313-321.

Foster, R.C. (2009), "Boundary-layer similarity under an axisymmetric, gradient wind vortex", *Bound. – Lay. Meteorol*., **131**(3), 321-344.

Giammanco, I.M., Schroeder, J.L. and Powell, M.D. (2013), "GPS dropwindsonde and WSR-88D observations of tropical cyclone vertical wind profiles and their characteristics", *Weather Forecast*., **28**, 77-99.

Gray, W.M. (1991), "Comments on 'Gradient Balance in Tropical Cyclones", *J. Atmos. Sci*., **48**, 1201-1208.

Heo, B.H., Jacoby-Koaly, S., Kim, K., Campistron, B., Benech, B. and Jung, E. (2003), "Use of the Doppler spectral width to improve the estimation of the convective boundary layer height from UHF wind profiler observations", *J. Atmos. Oncean. Tech*., **20**, 408-424.

Hill, K.A. and Lackmann, G.M. (2009), "Analysis of idealized tropical cyclone simulations using the

weather research and forecasting model: Sensitivity to turbulence parameterization and grid spacing", *Mon. Weather Rev*., **137**, 745-765.
Holland, G.J. (1980) "An analytic model of the wind and pressure profiles in hurricanes", *Mon. Weather Rev*., **108**(8), 1212-1218.
Kepert, J. (2001), "The dynamics of boundary layer jets within the tropical cyclone core. Part I: Linear theory", *J. Atmos. Sci*., **58**(17), 2469-2484.
Kepert, J. (2006a), "Observed boundary layer wind structure and balance in the hurricane core. Part I: Hurricane Georges", *J. Atmos. Sci*., **63**(9), 2169-2193.
Kepert, J. (2006b), "Observed boundary layer wind structure and balance in the hurricane core. Part II: Hurricane Mitch", *J. Atmos. Sci* ., **63**(9), 2194-2211.
Powell, M.D., (1987), "Changes in the low-level kinematic and thermodynamic structure of Hurricane Alicia (1983) at landfall", *Mon. Weather Rev*., **115**(1), 75-99.
Powell, M.D., Uhlhorn, E.W. and Kepert, J.D. (2009), "Estimating maximum surface winds from hurricane reconnaissance measurements", *Weather Forecast*., **24**(3), 868-883.
Shapiro, L.J. (1983), "The asymmetric boundary layer flow under a translating hurricane", *J. Atmos. Sci*., **40**(8), 1984-1998.
Smith, R.K. (1968), "The surface boundary layer of a hurricane", *Tellus*, **20**, 473-484.
Smith, R.K. and Montgomery M.T. (2008), "Balanced boundary layers used in hurricane models", *Q. J. Roy. Meteorol. Soc*., **134**(635), 1385-1395.
Thomas, P. and Vogt, S. (1993), "Variances of the vertical and horizontal wind measured by tower instruments and SODAR", *Appl. Physics B*, **57**, 19-26.
Tse, K.T., Li, S., Chan, P.W., Mok, H.Y. and Weerasuriya, A.U. (2013), "Wind profile observations in tropical cyclone events using boundary layer wind-profilers and doppler SODARs", *J. Wind Eng. Ind. Aerod*., **115**, 93-103.
Vickery, P.J., Wadhera, D., Powell, M.D. and Chen, Y. (2009), "A hurricane boundary layer and wind field model for use in engineering applications", *J. Appl. Meteorol. Clim*., **48**(2), 381-405.
Wang, Y. and Wu, C.C. (2003), "Current understanding of tropical cyclone structure and intensity changes–a review", *Meteorol. Atmos. Phys*., **87**(4), 257-278.
Willoughby, H.E. (1990), "Gradient balance in tropical cyclones", *J. Atmos. Sci*., **47**(2), 265-274.
Yeung, L.H., Chan, P.K.Y. and Lai, E.S.T. (2005), "Impact of radar rainfall data assimilation on short-range quantitative precipitation forecasts using four-dimensional variational analysis technique", *Proceedings of the 11th AMS Conference on Mesoscale Processes*, Albuquerque, New Mexico.

JH